


# Silencing of *OsCV* (*chloroplast vesiculation*) maintained photorespiration and N assimilation in rice plants grown under elevated CO<sub>2</sub>

Kamolchanok Umnajkitikorn<sup>1,2</sup> | Nir Sade<sup>3</sup> | Maria del Mar Rubio Wilhelmi<sup>1</sup> | Matthew E. Gilbert<sup>1</sup> | Eduardo Blumwald<sup>1</sup> 

<sup>1</sup>Department of Plant Sciences, University of California, Davis, CA

<sup>2</sup>School of Crop Production Technology, Institute of Agricultural Technology, Nakhon Ratchasima, Thailand

<sup>3</sup>Department of Molecular Biology & Ecology of Plants, Faculty of Life Sciences, Tel Aviv University, Tel Aviv, Israel

## Correspondence

Eduardo Blumwald, Department of Plant Sciences, University of California, Davis, CA 95616.  
Email: eblumwald@ucdavis.edu

## Funding information

MARI, MARS Advanced Research Institute; Will W. Lester Endowment, University of California

## Abstract

High CO<sub>2</sub> concentrations stimulate net photosynthesis by increasing CO<sub>2</sub> substrate availability for Rubisco, simultaneously suppressing photorespiration. Previously, we reported that silencing the *chloroplast vesiculation* (*cv*) gene in rice increased source fitness, through the maintenance of chloroplast stability and the expression of photorespiration-associated genes. Because high atmospheric CO<sub>2</sub> conditions diminished photorespiration, we tested whether CV silencing might be a viable strategy to improve the effects of high CO<sub>2</sub> on grain yield and N assimilation in rice. Under elevated CO<sub>2</sub>, *OsCV* expression was induced, and *OsCV* was targeted to peroxisomes where it facilitated the removal of OsPEX11-1 from the peroxisome and delivered it to the vacuole for degradation. This process correlated well with the reduction in the number of peroxisomes, the decreased catalase activity and the increased H<sub>2</sub>O<sub>2</sub> content in wild-type plants under elevated CO<sub>2</sub>. At elevated CO<sub>2</sub>, CV-silenced rice plants maintained peroxisome proliferation and photorespiration and displayed higher N assimilation than wild-type plants. This was supported by higher activity of enzymes involved in NO<sub>3</sub><sup>-</sup> and NH<sub>4</sub><sup>+</sup> assimilation and higher total and seed protein contents. Co-immunoprecipitation of *OsCV*-interacting proteins suggested that, similar to its role in chloroplast protein turnover, *OsCV* acted as a scaffold, binding peroxisomal proteins.

## KEYWORDS

chloroplast vesiculation, elevated CO<sub>2</sub>, nitrogen assimilation, peroxisomes, photorespiration

## 1 | INTRODUCTION

A range of anthropogenic factors is rapidly increasing atmospheric CO<sub>2</sub>, causing significant changes in global temperature and thereby precipitation patterns (Gamage et al. 2018). Since the industrial revolution, global atmospheric CO<sub>2</sub> concentrations have increased rapidly, rising from 280 to 400 ppm (Tans & Keeling, 2016; Thompson, Gamage, Hirotsu, Martin, & Saman, 2017). CO<sub>2</sub> directly affects plant metabolism in general and photosynthesis in particular (Dusenge, Duarte, & Way, 2018). Ribulose-1,5-bisphosphate carboxylase/oxygenase (Rubisco) is the key enzyme in the photosynthetic process,

catalysing two inseparable chemical reactions: (a) carboxylation or Calvin-Benson reaction, where a five-carbon sugar RuBP (ribulose-1,5-bisphosphate) is combined with CO<sub>2</sub> to produce two molecules of glycerate-3-phosphate; and (b) oxygenation or photorespiration pathway, a combination of RuBP with O<sub>2</sub>, that yields one molecule of glycerate-3-phosphate and one molecule of phosphoglycolate. Higher CO<sub>2</sub> concentrations will stimulate net photosynthesis by increasing CO<sub>2</sub> substrate availability for Rubisco, simultaneously suppressing photorespiration (Drake, González-Meler, & Long, 1997). Thus, high CO<sub>2</sub> will increase photosynthesis, improving carbohydrate production (i.e., positive for growth and yield in crops), but will also cause several

negative effects as carbon–nitrogen imbalance and/or decrease in the number of grana-thylakoid structures (Cao, Jiang, Xu, Liu, & Meng, 2017; Teng et al., 2006). Although photorespiration induces a reduction in CO<sub>2</sub> assimilation, it provides protection of leaves during stress by dissipating excess reducing equivalents and energy, that is, adenosine triphosphate, NAD(P)H, and reduced ferredoxin (Voss, Sunil, Scheibe, & Raghavendra, 2013). Moreover, photorespiration has been proposed as a necessary pathway for N assimilation in C3 plants under elevated atmospheric CO<sub>2</sub> (Bloom, 2015).

During photorespiration, peroxisomal and mitochondrial enzymes cooperate to convert glycolate, produced in the chloroplast, to glycerate to be recycled to the chloroplast for the Calvin–Benson cycle. Glycolate oxidases, active during photorespiration, contribute to the accumulation of peroxisomal H<sub>2</sub>O<sub>2</sub>, which is broken down into water and molecular oxygen by the action of catalases in the peroxisome (Timm et al., 2013). In addition to photorespiration, peroxisomes are involved in several catabolic and biosynthetic reactions, such as reactive oxygen species production and detoxification, hormones synthesis, and fatty acids  $\beta$ -oxidation (Kao, Gonzalez, & Bartel, 2018). Peroxisomes are highly dynamic organelles, able to adjust their size and number in response to environmental, developmental, and metabolic factors. Peroxisomal fission and proliferation are controlled by the peroxisome biogenesis factors PEROXIN11 (PEX11) protein family and several transcription factors (Reumann & Bartel, 2016). Although peroxisome functions are crucial in cell metabolism, the processes regulating peroxisomal dynamics are not clear in plants (Kao et al., 2018; Kessel-Vigelius et al., 2013).

The nuclear gene *chloroplast vesiculation* (*cv*) encodes a protein that plays a key role in the destabilization of the photosynthetic apparatus during senescence and abiotic stress (Wang & Blumwald, 2014). Upon stress, CV interacts with thylakoid membrane-bound proteins (i.e., PsbO1 in photosystem [PS]II and CYP20 in PSI) and stromal proteins (i.e., chloroplastic glutamine synthetase, GS2), inducing the formation of vesicles. CV-containing vesicles mobilize thylakoid and stroma proteins to the vacuole for degradation through a pathway that is independent of autophagy and senescence-associated vacuoles (Wang & Blumwald, 2014; Sade et al., 2018). Previous work in Arabidopsis and rice showed that CV silencing was a valuable strategy to increase the tolerance of plants to water deficit through the maintenance of chloroplast integrity; rice CV-silenced plants (*Oscv*) displayed enhanced source fitness, maintaining chloroplast stability and affecting N cytosolic assimilation through the regulation of nitrate reductase (NR) (Sade et al., 2018). In addition, under water deficit, *Oscv* displayed the enhanced expression of genes associated with photorespiration (Sade et al., 2018). It is well established that in C3 plants, enhancing photorespiration resulted in an increased N assimilation via NR (Bloom, 2015; Rachmilevitch, Cousins, & Bloom, 2004). However, the relationship between CV, the photorespiratory pathway, and NR-mediated N assimilation is not yet clear.

Here, we show that under high CO<sub>2</sub> atmospheric conditions (with the concomitant decrease in photorespiration), OsCV directly interacted with OsPEX11-1 in the peroxisome. The interaction between these proteins was maintained during trafficking to the prevacuolar

compartment (PVC) and to the vacuole. Our results indicated the role of OsCV in mediating peroxisomal turnover, contributing to the regulation of photorespiration and N assimilation in rice plants under elevated CO<sub>2</sub>.

## 2 | MATERIALS AND METHODS

### 2.1 | Plant material and growth conditions

Seeds of wild-type (WT) rice (*Oryza sativa japonica* “Kitaake”) and two independent lines of transgenic RNAi-OsCV plants (Sade et al., 2018) were germinated on moist germination paper for 10 days at 28°C in the dark. Seedlings were transplanted into 1.25-L pots filled with 8-mm expanded clay aggregate pebble pellets (Hydro Crunch, Walnut, CA, USA). The seedlings were grown at ambient conditions (12-hr/12-hr day/night and 28°C/20°C 800  $\mu\text{mol m}^{-2} \text{s}^{-1}$ ) in the greenhouse for 7 days and then transferred to growth chambers with ambient CO<sub>2</sub> (440–450 ppm) or elevated CO<sub>2</sub> (700 ppm) with a 12-hr/12-hr day/night at 28°C/20°C and 800  $\mu\text{mol m}^{-2} \text{s}^{-1}$  of photosynthetically active radiation and relative humidity controlled between 40% and 50%. Plants were fertilized weekly with (N: 75 ppm, P: 20 ppm, K: 75 ppm, Ca: 25 ppm, Mg: 17 ppm, S: 55 ppm, Fe: 3.30 ppm, Mn: 0.50 ppm, Zn: 0.05 ppm, Mo: 0.01 ppm, and Cu: 0.02 ppm) for 3 weeks. Nitrogen in the fertilizer was supplied equally in the forms of KNO<sub>3</sub> and (NH<sub>4</sub>)<sub>2</sub>SO<sub>4</sub>. Leaf samples for RNA, biochemical assays, and gas exchange measurements were taken after 3 weeks of growth in the chambers. The leaves were collected in the morning, between 10.30 and 11.30 a.m. (1.30–2.30 hr after the light turned on) and immediately frozen in liquid nitrogen and kept at –80°C until use.

### 2.2 | Constructs and generation of transgenic plants

All the constructs in this study were generated using the Gateway cloning system (Invitrogen, Carlsbad, CA, USA).

#### 2.2.1 | RNAi-OsCV and EST::OsCV plants

The constructs and transgenic plants were generated as described previously (Sade et al., 2018).

#### 2.2.2 | Bimolecular fluorescence complementation

The vectors *pDEST-GWVYNE* and *pDEST-GWSCYCE* from the Gateway-based bimolecular fluorescence complementation (BiFC) vector systems (Gehl, Waadt, Kudla, Mendel, & Hänsch, 2009) were employed to fuse OsCV (LOC\_Os05g49940) and OsPEX11-1 (LOC\_Os03g02590) with the C-terminus of super cyan fluorescent protein (SCFP<sup>C</sup>) or the N-

terminus of yellow fluorescent protein Venus (Venus<sup>N</sup>) to obtain the constructs OsCV-SCFP<sup>C</sup> and OsPEX11-1-Venus<sup>N</sup>.

### 2.2.3 | In vivo OsCV and OsPEX11-1 interaction and colocalization

For protein colocalization assays, the open reading frame of OsCV, excluding the stop codon, was amplified from mature leaf cDNA and cloned into *pDONR207* and the destination vector *pEarleyGate 102* (Earley et al., 2006) for CFP fusion. Using the same strategy, OsPEX11-1 was fused with yellow fluorescent protein (YFP) of *pEarleyGate 101*. All the constructs were introduced into *Agrobacterium tumefaciens* GV3101. Transient expression was performed in leaves of *Nicotiana benthamiana* as described previously (Li, 2011).

### 2.3 | Gas exchange measurements

Rubisco carboxylation rate ( $V_c$ ) and oxygenation rate ( $V_o$ ) measurements were recorded in intact plants using a Li-6,400 portable gas exchange system (LI-COR, Nebraska, USA). Photosynthesis was induced by saturating light ( $1,200 \mu\text{mol m}^{-2} \text{s}^{-1}$ ) with  $700 \mu\text{mol mol}^{-1}$  or  $350 \mu\text{mol mol}^{-1}$  CO<sub>2</sub> surrounding the leaf ( $C_a$ ) with or without modifications of O<sub>2</sub> concentrations. Relative humidity was around 40–50%.  $V_o$  was measured at 2% oxygen (balanced with nitrogen; Praxair, Sacramento, CA, USA). The amount of blue light was set to 10% of photosynthetically active photon flux density (PPFD) to optimize stomatal aperture. Block temperature was set to 28°C. Photosynthesis was measured every 10 s for 30 s (the three data points were then averaged).  $V_c$  and  $V_o$  were calculated as described before (Ripley, Gilbert, Ibrahim, & Osborne, 2007).

A second experiment was performed to confirm the first (data shown in Figure S1). Plants were grown in the greenhouse, conditions were kept at 12-hr/12-hr day/night and 28°C/20°C, under normal and elevated CO<sub>2</sub> conditions. Photosynthesis and rubisco oxygenation activity were measured as described above with the following differences: measurements were made at two CO<sub>2</sub> concentrations optimized to be able to resolve photorespiration; “ambient”: 350 ppm and “elevated” 500 ppm. PPFD was  $500 \mu\text{mol m}^{-2} \text{s}^{-1}$  and leaf temperature averaged  $27.6 \pm 0.78^\circ\text{C}$ . Relative humidity was not controlled and varied from 22 to 42%; flow was set to  $250 \mu\text{mol s}^{-1}$ . Dark respiration ( $R_{\text{dark}}$ ) was estimated by measuring dark respiration at 21% O<sub>2</sub> following the photosynthesis measurements.

Chlorophyll fluorescence measurements ( $\Phi_{\text{PSII}}$ ) were made simultaneously to the gas exchange using the LI-COR6400 “multiphase flash” routine to estimate maximum fluorescence. These measurements were used to estimate a correction factor for oxygenation based upon that proposed by Bellasio, Burgess, Griffiths, and Hibberd (2014). Thus,  $V_o$  was corrected by the ratio of  $\Phi_{\text{PSII}}$  change with oxygen concentration, that is, the change in total electron transport through PSII as a result of the O<sub>2</sub> change:

$$V_{o,\text{corrected}} = \frac{2}{3} \left( A_{2\%} \frac{\Phi_{\text{PSII } 21\%}}{\Phi_{\text{PSII } 2\%}} - A_{21\%} \right),$$

where  $A_{2\%}$  and  $A_{21\%}$  are the gross assimilation rates at the respective O<sub>2</sub> concentrations (calculated as net assimilation + dark respiration).  $V_o$  was also estimated using the approach of Valentini, Epron, Angelis, Matteucci, and Dreyer (1995) as

$$V_{o,\text{Valentini}} = \frac{2}{3} (J_{\text{total}} - 4(A_{21\%})),$$

where  $J_{\text{total}}$ , the total electron transport through PSII, was estimated per Genty, Briantais, and Baker (1989) as  $\Phi_{\text{PSII},21\%} \times 0.85 \times 0.5 \times \text{PPFD}$ . This approach assumes that alternative electron sinks are negligible.

### 2.4 | Quantitative PCR analysis

RNA was extracted from youngest fully expanded leaves of WT and transgenic rice plants grown under ambient and elevated CO<sub>2</sub>. The different sets of primers used for the amplification of the target genes are listed in Table S1. Analysis of the relative gene expression was performed according to the comparative cycle threshold ( $2^{-\Delta\Delta\text{CT}}$ ) method (Livak & Schmittgen, 2001) and calibrated using transcript values relative to the endogenous rice transcription elongation factor gene (Reguera et al., 2013; Sade et al., 2018; Tamaki et al., 2015). There were no significant differences in expression of the examined genes under ambient conditions (data not shown). Therefore, for simplicity, results are presented only for elevated CO<sub>2</sub>.

### 2.5 | Metabolite profiling

Ground frozen powder of the youngest fully expanded leaves was submitted to the West Coast Metabolomics Center (University of California, Davis), extracted, measured, and analysed by gas chromatography–mass spectrometry (MS) (Gerstel CIS4–with a dual MPS Injector/Agilent 6,890 GC-Pegasus III TOF MS) as described before (Weckwerth, Wenzel, & Fiehn, 2004). Processes for the integrated extraction, identification, and quantification of metabolites were performed according to Fiehn et al. (2008). For the extraction, solvent was prepared by mixing isopropanol/acetonitrile/water at the volume ratio 3:3:2 and degassing the mixture by directing a gentle stream of nitrogen through the solvent for 5 min. Solvent (cooled at  $-20^\circ\text{C}$ ) was added to the ground tissue (1-ml solvent/20-mg tissue), vortexed, and shaken for 5 min for metabolite extraction. After centrifugation at 12,800 g for 2 min, supernatant was concentrated to dryness. The residue was resuspended in 0.5-ml 50% aqueous acetonitrile and centrifuged at 12,800 g for 2 min. The supernatant was concentrated to dryness in a vacuum concentrator, and the dried extracts were stored at  $-80^\circ\text{C}$  until use. Untargeted metabolomic analysis was used. The signals were normalized with the sum of all peak heights of the annotated detected metabolites as suggested by

Fiehn et al. (2008). No internal standard was added in the analysis. The equation used in this calculations was (for metabolite *i* of sample *j*) metabolite  $_{ij,normalized} = \text{metabolite}_{ij,raw} / \text{mTIC}_j * \text{mTIC}_{average}$ .

## 2.6 | Enzyme assays

Enzyme activities were determined in youngest fully expanded leaves of WT and transgenic plants exposed to ambient and elevated CO<sub>2</sub>. The leaves were collected in the morning (9–10 a.m.). Whole leaves from each plant were ground with liquid nitrogen, and the powder was aliquoted and stored at –80°C until use. Enzyme activities are expressed as moles of metabolite generated/consumed per milligram of protein per unit of time. NR and GS activities were measured according to Kaiser and Lewis (1984) with some modifications (Sade et al., 2018) and O'Neal and Joy (1973), respectively. CAT activity was determined by following the consumption of H<sub>2</sub>O<sub>2</sub> (extinction coefficient 39.4 mM<sup>-1</sup> cm<sup>-1</sup>) at 240 nm for 1 min (Aebi, 1984). The reaction mixture contained 50-mM potassium phosphate buffer (pH 7.0), 10 mM H<sub>2</sub>O<sub>2</sub> and 50 μl of enzyme extract in a 1-ml volume. The Bradford assay (Bradford, 1976) was used for protein quantification using bovine serum albumin as a standard.

## 2.7 | H<sub>2</sub>O<sub>2</sub> quantification

The frozen leaves were ground, and 5–10 mg of samples were extracted with 1 ml of 20-mM K<sub>2</sub>HPO<sub>4</sub> (pH 6.5), homogenized for 5 min at 4°C, and then centrifuged for 3 min at 16,200 g at 4°C. The H<sub>2</sub>O<sub>2</sub> detection assay by Amplex Red (Thermo Fisher Scientific, Waltham, MA, USA) was performed on the supernatant, as described in Brumbarova, Le, and Bauer (2016) with some modifications, that is, the reaction was incubated for 15 min instead of 30 min.

## 2.8 | <sup>15</sup>N analysis

Plants were grown as described above with or without (control) substitution of either KNO<sub>3</sub> or (NH<sub>4</sub>)<sub>2</sub>SO<sub>4</sub> with 4% atom K<sup>15</sup>NO<sub>3</sub> or (<sup>15</sup>NH<sub>4</sub>)<sub>2</sub>SO<sub>4</sub> (Cambridge Isotope Laboratories, Inc. Tewksbury, MA, USA) to yield a 2% atom <sup>15</sup>N at the final concentration for 2 weeks before the sample collection. The youngest fully expanded leaves were collected from WT and RNAi-OsCV rice plants and dried in an oven at 80°C for 7 days before grinding. Samples (2–4 mg) of powder were sent to the University of California, Davis, Stable Isotope Facility for <sup>15</sup>N analysis. Plant samples were analysed for <sup>15</sup>N isotopes using an Elementar Micro Cube elemental analyser (Elementar Analysensysteme GmbH, Hanau, Germany) interfaced to a PDZ Europa 20–20 isotope ratio mass spectrometer (Sercon Ltd., Cheshire, UK). Samples are combusted at 1,000°C in a reactor packed with chromium oxide and silvered copper oxide. Following combustion, oxides were removed in a reduction reactor (reduced copper at 650°C). The helium carrier then flowed through a water trap (magnesium perchlorate and

phosphorous pentoxide). CO<sub>2</sub> was retained on an adsorption trap until the N<sub>2</sub> peak was analysed; the adsorption trap was then heated releasing the CO<sub>2</sub> to the IRMS.

During analysis, samples were interspersed with several replicates of at least four different laboratory reference materials. Natural abundance reference materials have been previously calibrated against international reference materials, including IAEA-600, USGS-40, USGS-41, USGS-42, USGS-43, USGS-61, USGS-64, and USGS-65. Because no highly enriched <sup>15</sup>N references exist, <sup>15</sup>N values for enriched laboratory references have been established by multiple isotope dilutions. A sample's provisional isotope ratio was measured relative to a reference gas peak analysed with each sample. These provisional values were finalized by correcting the values for the entire batch based on the known values of the included laboratory reference materials. For natural abundance samples, the long-term standard deviation was 0.2 per mil for <sup>13</sup>C and 0.3 per mil for <sup>15</sup>N. Because there were no significant differences in the expression of the examined genes from plants grown under ambient and elevated CO<sub>2</sub> conditions (data not shown), for simplicity, only the results obtained from plants under elevated CO<sub>2</sub> conditions are presented.

## 2.9 | NO<sub>3</sub><sup>-</sup> and NH<sub>4</sub><sup>+</sup> contents

Ground dried leaf tissue (100 mg) was used for NH<sub>4</sub><sup>+</sup> and NO<sub>3</sub><sup>-</sup> quantification. For the measurement of NH<sub>4</sub><sup>+</sup> tissue content, the tissue was agitated for 2 hr in 2-M KCl. After filtration, NH<sub>4</sub><sup>+</sup> was determined as described according to Krom (1980). NO<sub>3</sub><sup>-</sup> was determined according to Zhao and Wang (2017).

## 2.10 | Electron microscopy

For standard transmission electron microscopy, the youngest fully expanded leaves were fixed in Karnovsky's fixative (2.0% paraformaldehyde and 2.5% glutaraldehyde; Electron Microscopy Sciences, Hatfield, PA) in 0.1-M sodium phosphate buffer, pH 7.4. Samples were post-fixed with 1% OsO<sub>4</sub> in the same buffer. Ultrathin cross-sections (70 nm) of the rice mesophyll cells were obtained using a Leica Ultracut UCT ultramicrotome and stained with uranyl acetate followed by lead citrate. The samples were observed with a Philips CM120 Biotwin lens (F.E.I.).

## 2.11 | Immunolabeling transmission electron microscopy

Fourteen-day-old seedlings of *EST::OsCV*-green fluorescent protein (GFP) transgenic plants and Col-0 were sprayed with 50-μM β-estradiol 24 hr before sampling. The induced leaves were fixed in 4% paraformaldehyde and 0.1% glutaraldehyde in 0.1-M sodium phosphate buffer. Co-immunolabeling was performed on ultrathin sections on Formvar-coated grids using a mouse anti-GFP monoclonal

antibody (Novus Biologicals, Littleton, CO, USA) and a rabbit anti-GOX (Agriseria, Vännäs, Sweden) antibody and then labeled with a goat anti-mouse secondary antibody conjugated with 10-nm gold particles (Electron microscopy sciences, Hatfield, PA, USA) and a goat anti-rabbit secondary antibody conjugated with 20-nm gold particles (Abcam, Cambridge, MA, USA). All the grids were stained with uranyl acetate and lead citrate before being observed on a Philips CM120 Biotwin. Images were taken with a Gatan MegaScan digital camera (Model 794/ 20).

## 2.12 | Immunoblot analyses

The youngest fully expanded leaf tissues were weighed, frozen in liquid N<sub>2</sub>, and ground in three volumes of extraction buffer (50-mM HEPES, 100-mM NaCl, 10-mM KCl, and 0.4-M sucrose) containing 1-mM PMSF and 1% of protease inhibitor cocktail (Sigma-Aldrich, St. Louis, MO, USA). Total proteins were denatured by mixing with Laemmli sample buffer, then separated by SDS-PAGE, transferred to a polyvinylidene difluoride membrane (Bio-Rad, Hercules, CA, USA), and probed as described previously (Wang et al., 2011). Antibodies raised against NR and GS were obtained from Agriseria (Vännäs, Sweden).

Horseradish peroxidase-conjugated secondary antibodies were purchased from Santa Cruz Biotechnology (Dallas, TX, USA).

## 2.13 | Fluorescence and confocal microscopy

Fluorescence microscopy was performed using an inverted Zeiss LSM 710 confocal laser scanning microscope (Carl Zeiss, Oberkochen, Germany) equipped with a 40× water immersion objective. The excitation/emission wavelengths were as follows: GFP (488 nm/500 to 530 nm), YFP (514 nm/ 527 to 572 nm), CFP (405 nm/ 463 to 498 nm), red fluorescent protein (RFP) (561 nm/600 to 660 nm), and chlorophyll (633 nm/650 to 720 nm).

## 2.14 | Immunoprecipitation and LC-MS/MS

One-week-old seedlings of WT and transgenic *EST::OsCV-GFP* were cultured in one half MS medium containing 20 μM of β-estradiol or 0.01% dimethyl sulfoxide for 24 hr. The plant shoots were harvested, ground in liquid N<sub>2</sub>, and incubated at 4°C for 4 hr with lysis buffer provided in the μMACS GFP isolation kit (Miltenyl Biotec, Bergisch

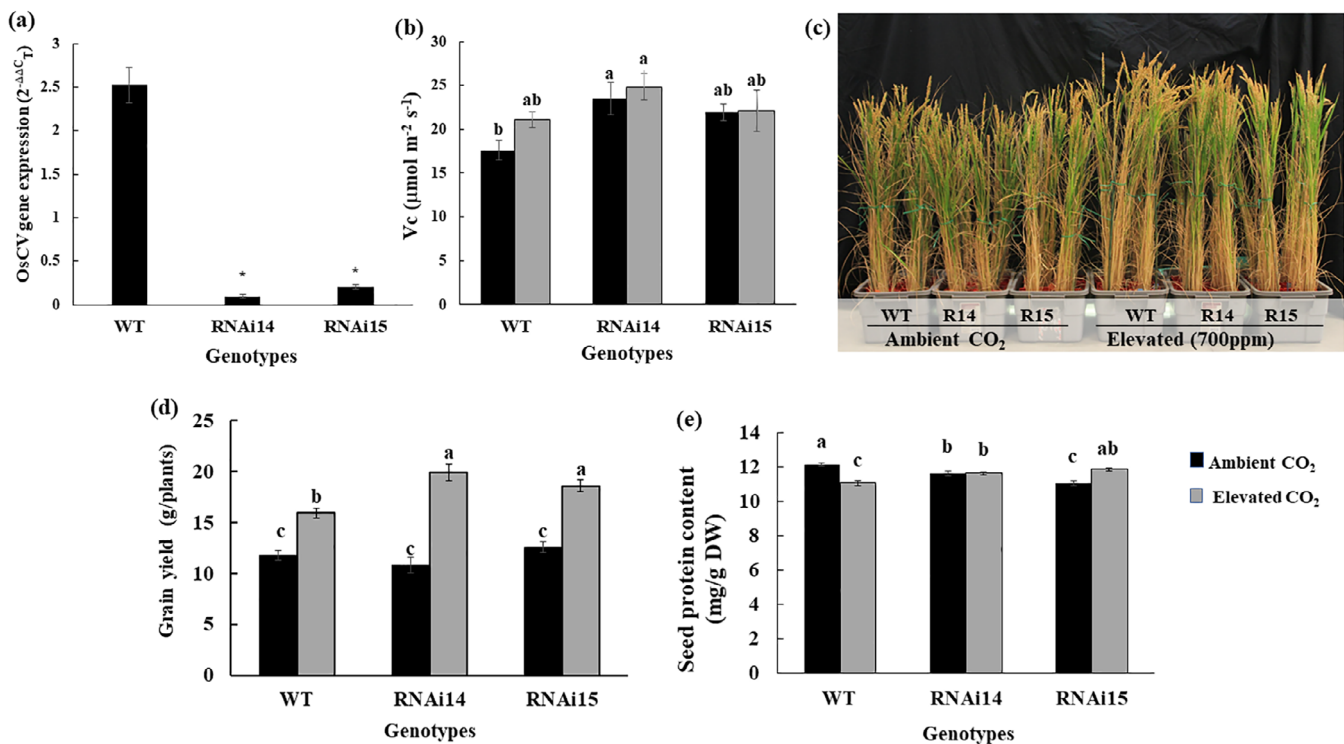


**FIGURE 1** OsCV expression and growth of wild-type (WT) and CV-silenced rice under elevated CO<sub>2</sub>. (a) Quantitative RT-PCR analysis of OsCV gene expression in the youngest fully expanded leaves of wild type and two independent lines of transgenic RNAi-OsCV plants (RNAi14 and RNAi15) in response to elevated CO<sub>2</sub>, relative to OsCV expression of WT plants grown under ambient CO<sub>2</sub>. Values are the mean ± standard error ( $n = 5$ ). The asterisks indicate significant differences by Student's  $t$ -test ( $p \leq .05$ ). (b) Carboxylation rate of Rubisco ( $V_c$ ) of WT and RNAi-OsCV plants under ambient and elevated CO<sub>2</sub>. Growth (c), grain yield (d), and seed protein content (e) of WT and transgenic CV-silenced rice plants under ambient CO<sub>2</sub> and elevated CO<sub>2</sub> (700 ppm). Values are the mean ± standard error ( $n = 6, 12, \text{ and } 5$ , respectively). The different letters above the bars indicate significant differences by one-way analysis of variance and Duncan's test ( $p \leq .05$ )



Gladbach, Germany), containing 1% protease inhibitor cocktail (Sigma-Aldrich, St. Louis, MO, USA), and 1 mM PMSF. Co-immunoprecipitation was performed using anti-GFP magnetic beads from the  $\mu$ MACS GFP isolation kit (Miltenyi Biotec, Santa Barbara, CA), and cell lysis was incubated with beads at 4°C for 4 hr. Liquid chromatography (LC)-MS/MS analysis was performed as described previously (Shipman-Roston, Ruppel, Damoc, Phinney, & Inoue, 2010). Scaffold (version Scaffold 4; www.proteomesoftware.com) was used to validate tandem MS-based peptide and protein identification. The results were filtered with a false discovery rate of less than 0.5% on the peptide level and 1% on the protein level with a minimum of two unique peptides required for identification (Fan et al., 2016).

## 2.15 | Statistical analysis

The SPSS 25 statistical package was used for statistical analyses. The experiments were based on a randomized complete block design.

## 3 | RESULTS

### 3.1.1 | OsCV silencing induced grain yield increase and high seed protein content in rice plants grown under elevated CO<sub>2</sub>

High atmospheric CO<sub>2</sub> concentrations inhibit both photorespiration and shoot nitrate assimilation, with the associated decrease in plant protein contents (Bloom, Burger, Asensio, & Cousins, 2010). We have shown previously that OsCV-mediated chloroplast degradation was associated with the regulation of nitrogen assimilation during stress-induced senescence (Sade et al., 2018). We assessed whether the silencing of CV would improve plant growth under elevated CO<sub>2</sub>. OsCV expression was induced by elevated CO<sub>2</sub>, whereas OsCV expression in transgenic RNAi-CV plants was reduced to 3–5% of that of WT plants (Figure 1a). Although not significant, WT plants showed an increase in the rate of carboxylation by Rubisco, whereas the CV silencing did not affect this rate under high level of atmospheric CO<sub>2</sub>

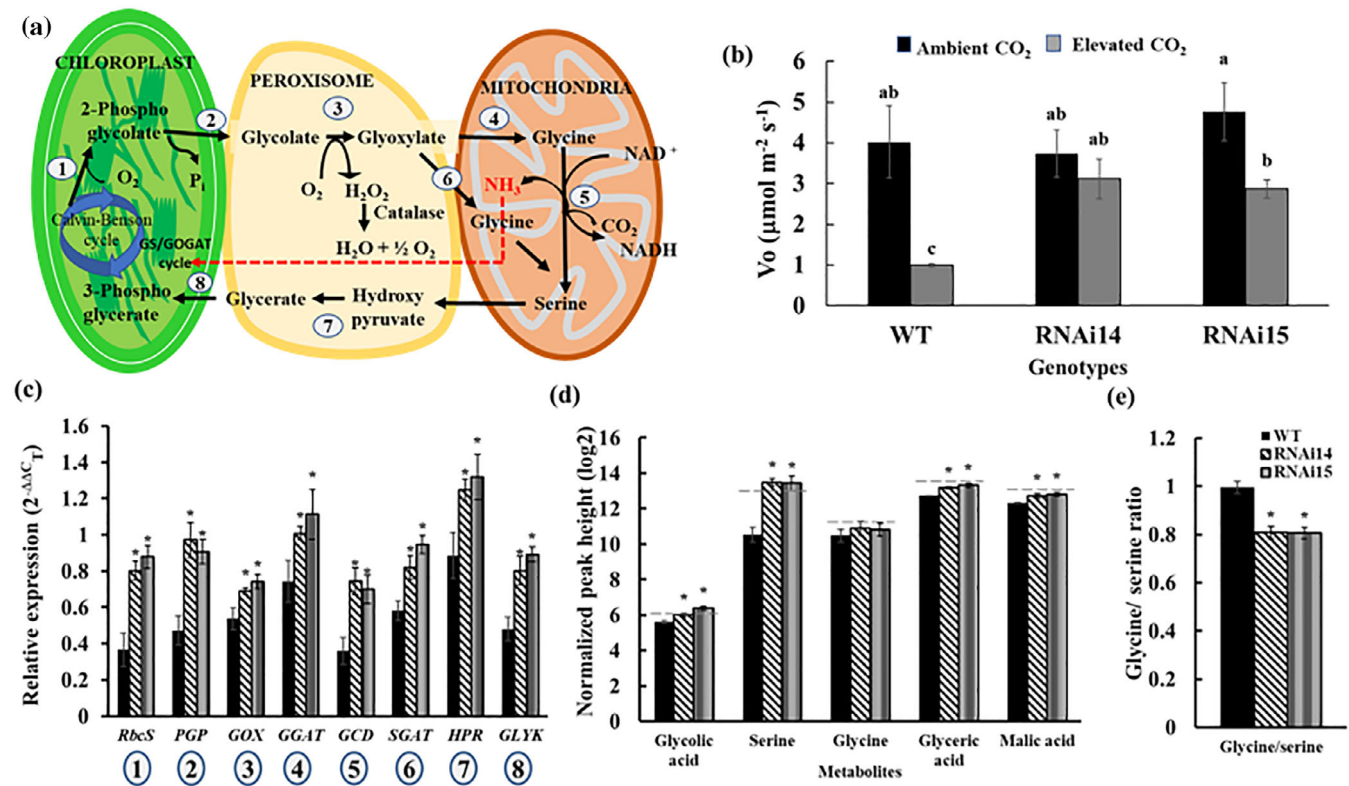


**FIGURE 2** CV-silenced rice maintained a higher photorespiration under elevated CO<sub>2</sub>. (a) A schematic representation of the photorespiratory pathway of C<sub>3</sub> plants. 1, rubisco small subunit (RbcS); 2, 2-phosphoglycolate phosphatase (PGP); 3, glycolate oxidase (GOX); 4, glutamate: glyoxylate aminotransferase (GGAT); 5, glycine decarboxylase (GCD); 6, serine: glyoxylate aminotransferase (SHMT); 7, NAD<sup>+</sup> hydroxypyruvate reductase (HPR); 8, glycerate kinase (GLYK). (b) photorespiration rate (V<sub>o</sub>) of wild-type (WT) and RNAi-OsCV plants under ambient and elevated CO<sub>2</sub>. Values are the mean ± standard error (SE; n = 6). (c) Relative expression of selected transcripts associated with photorespiration (1–8 as shown in panel a) of WT and RNAi-OsCV plants under elevated CO<sub>2</sub>. Values are the mean ± SE (n = 5). The asterisks indicate significant differences by Student's *t*-test (*p* ≤ .05). (d) Selected metabolite contents of WT and RNAi-OsCV plants under elevated CO<sub>2</sub>. The dashed line represents the value of each metabolite under ambient conditions. Values are the mean ± SE (n = 4). (e) Glycine:serine ratio of WT and RNAi-OsCV plants grown under elevated CO<sub>2</sub>. Values are the mean ± SE (n = 4), and the asterisks indicate significant differences by Student's *t*-test (*p* ≤ .05). The different letters above the bars indicate significant differences by one-way analysis of variance and Duncan's test (*p* ≤ .05)

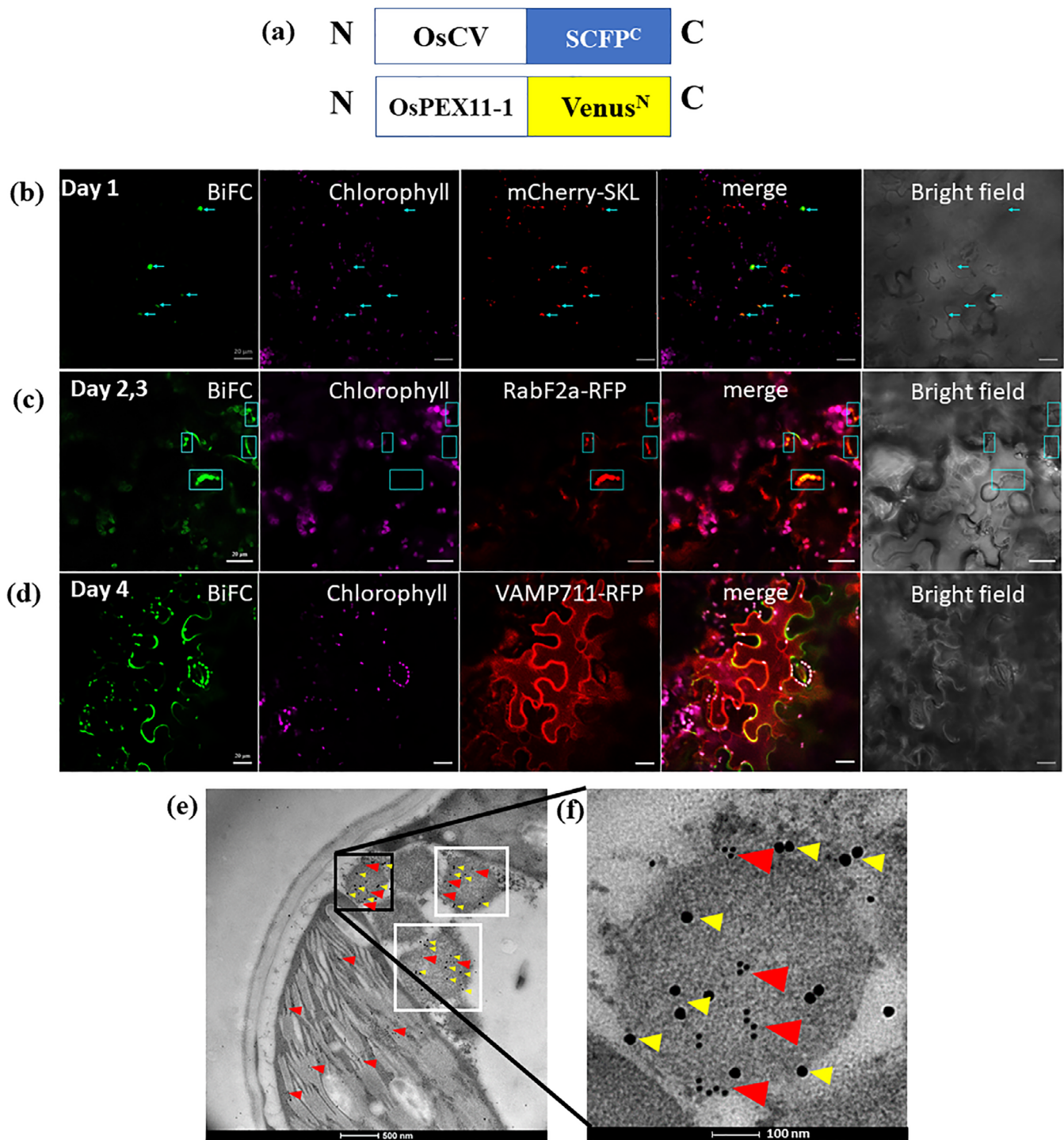


**FIGURE 3** OsCV has a role in the mobilization of the peroxisomal biogenesis factor 11 (OsPEX11-1) from peroxisome to vacuoles. (a) Bimolecular fluorescence complementation (BiFC) design: SCFP<sup>C</sup> and Venus<sup>N</sup> were fused at the C-terminus of OsCV and OsPEX11-1, respectively. (c-d) BiFC analysis of in vivo interactions between OsCV-SCFP<sup>C</sup> and OsPEX11-1-Venus<sup>N</sup> (CV + PEX11) by transient expression in *Nicotiana benthamiana*. (b) BiFC signals obtained 1 day after infiltration. Most of the signals overlapped with the peroxisome marker mCherry-SKL (blue arrows). (c) BiFC signals obtained 2 to 3 days after infiltration. Signals overlapped with chloroplasts and the prevacuolar compartment marker RabF2a-RFP. (d) BiFC signals obtained 4 days after infiltration. Signals overlapped with the vacuolar marker VAMP711-RFP. (e-f) Co-immunodetection of CV-GFP and OsGOX (peroxisome marker) in peroxisomes. (e) EST-CV-GFP transgenic plants were induced by 50- $\mu$ M  $\beta$ -estradiol, labelled with anti-GFP mouse (10-nm gold particles, red arrows) and anti-GOX rabbit (20-nm gold particles, yellow arrows) and observed by immunolabeling transmission electron microscopy. Red arrows indicate OsCV presence in both chloroplast and peroxisomes. Black and white squares indicate CV localization in peroxisomes. (f) A higher magnification of the area from black square in (e)

(Figure 1b). High CO<sub>2</sub> enhanced plant growth in a similar manner in all genotypes (Figure 1c). Elevated CO<sub>2</sub> enhanced grain yield production in both WT and CV-silenced plants; however, the yield increase was significantly higher in CV-silenced plants than in WT (Figure 1d). Seed protein contents decreased in WT plants under elevated CO<sub>2</sub>, whereas it remained constant in CV-silenced plants (Figure 1e).

### 3.1.2 | OsCV silencing induced higher photorespiration under elevated CO<sub>2</sub>

When grown under elevated CO<sub>2</sub>, CV-silenced rice plants displayed higher Rubisco oxygenation ( $V_o$ ) than WT plants, which was similar to that grown under control conditions (Figure 2b). A second experiment optimized to measure oxygenation rates confirmed this pattern (Figure S1a). Gene expression and metabolite analyses of RNAi-OsCV rice plants grown under elevated CO<sub>2</sub> revealed the enhanced expression of photorespiration-associated genes (Figures 2b,c). The expression levels of genes encoding Rubisco small subunit (RbcS);

2-phosphoglycolate phosphatase (PGP), glycolate oxidase (GOX), glutamate:glyoxylate aminotransferase (GGAT), glycine decarboxylase (GCD), serine:glyoxylate aminotransferase (SHMT), NAD<sup>+</sup> hydroxypyruvate reductase (HPR), and glycerate kinase (GLYK) were significantly higher than WT grown under elevated CO<sub>2</sub>. Of the photorespiration pathway-associated metabolites tested, glycolate, serine, glycerate, and malic acid were higher in CV-silenced plants than in WT plants (Figure 2d). In addition, we calculated the glycine:serine ratio resulting significantly higher in WT compare with CV-silenced plants under high CO<sub>2</sub> conditions (Figure 2e).

### 3.1.3 | OsCV interacts in vivo with OsPEX11 (peroxisome biogenesis factor 11)

To elucidate the mechanism(s) by which OsCV might affect photorespiration, we identified putative CV-interacting proteins by co-immunoprecipitation and subsequent MS-based identification of the interacting proteins. Immunoprecipitated proteins interacting with

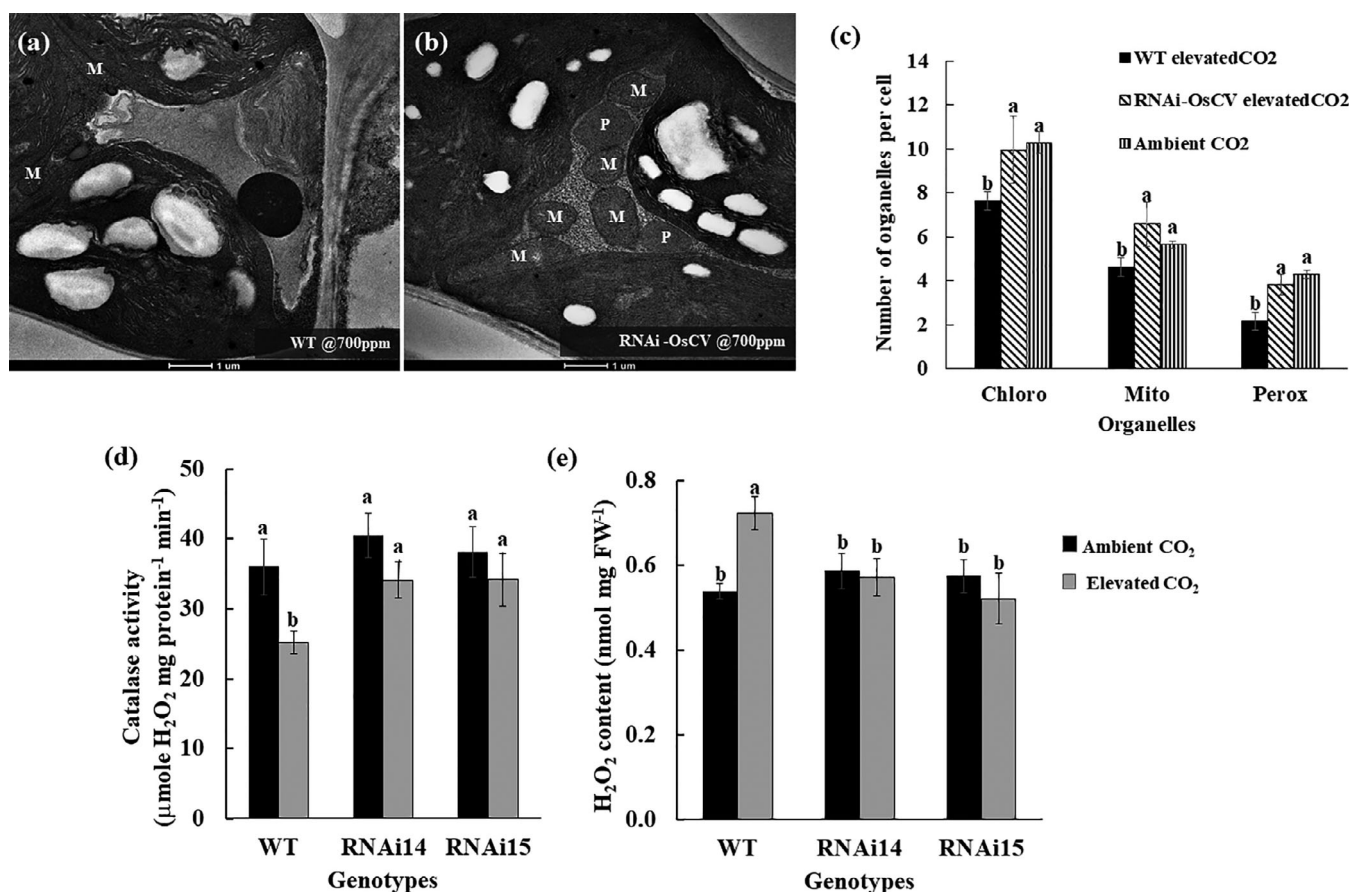


**FIGURE 4** CV silencing contributed to more coherence of organelles necessary for photorespiration and detoxification of H<sub>2</sub>O<sub>2</sub>. (a, b) Transmission electron micrographs showing the ultrastructure of WT (a) and RNAi-OsCV (b) leaf mesophyll cells, under elevated CO<sub>2</sub>. Organelles were labeled as M, mitochondria; P, peroxisomes. (c) Numbers of organelles involved in photorespiration of WT and RNAi-OsCV leaf mesophyll cells under elevated CO<sub>2</sub> as observed by transmission electron microscopy. Values are the mean ± standard error ( $n = 30$  cells from three different plants). The asterisks indicate significant differences by Student's  $t$ -test ( $p \leq .05$ ). (d–f) Catalase activity (d), H<sub>2</sub>O<sub>2</sub> content (e) and MDA content (f) of WT and RNAi-OsCV leaves under elevated CO<sub>2</sub>. Values are the mean ± standard error ( $n = 5$ ). The different letters above the bars indicate significant differences by one-way analysis of variance and Duncan's test ( $p \leq .05$ ). WT, wild type



O<sub>s</sub>CV-GFP were obtained from total protein extracts of  $\beta$ -estradiol-treated transgenic plants expressing inducible O<sub>s</sub>CV-GFP. Protein extracts from WT plants and *EST::CV-GFP* plants treated with dimethyl sulfoxide (no induction) were used as controls to identify proteins binding non-specifically to the anti-GFP beads. A number of peroxisome-associated proteins were identified by LC MS/MS only in the protein complexes obtained from *EST::CV-GFP* plants, among them the peroxisome biogenesis factor 11-1 (OsPEX11-1; Table S2). BiFC was used to confirm the O<sub>s</sub>CV-OsPEX11 interaction (Figure 3a). The transient expression of the fusion genes O<sub>s</sub>CV-SCFP<sup>C</sup> and OsPEX11-Venus<sup>N</sup> in *N. benthamiana* resulted in BiFC fluorescence (Figures 3b-d), confirming the *in vivo* interaction between O<sub>s</sub>CV and OsPEX11-1. The colocalization of the BiFC complex and mCherry-SKL fluorescence indicated the peroxisomal localization of the BiFC complex (Nelson, Cai, & Nebenfuhr, 2007), 1 day after induction (Figure 3b). To assess whether, similar to other protein degradation pathways, the O<sub>s</sub>CV/OsPEX11-1 complex was mobilized to the vacuoles, the BiFC constructs were transiently coexpressed with Rab2a-RFP, a PVC rab5 GTPase Rha1 (Foresti et al., 2010; Figure 3c) and VAMP711-RFP, encoding a tonoplast R-SNARE (Uemura, Tomonari, Kashiwagi, & Igarashi, 2004) in *N. benthamiana* leaves (Figure 3d). The CV-PEX11 BiFC complex was

transported through the endomembrane system to the PVC and vacuoles, as indicated by its colocalization with RabF2a-RFP after 2-3 days and with VAMP711-RFP after 4 days following infiltration, respectively (Figure 3c,d). We also transiently coexpressed CV-CFP together with PEX11-YFP in *N. benthamiana* leaves. Cells that coexpressed both CV-CFP and PEX11-YFP showed the colocalization of both proteins at peroxisomes (Figure S2a), PVCs (Figure S2b), and vacuoles (Figure S2c). In cells expressing only PEX11-YFP, PEX11-1 was mostly localized to peroxisomes 4 days after infiltration (Figure S2d). We further confirmed the localization of O<sub>s</sub>CV in peroxisomes by electron microscopy using gold-labeled O<sub>s</sub>CV-GFP and GOX (glycolate oxidase and peroxisome marker). In addition, O<sub>s</sub>CV was enriched in both at chloroplast thylakoid membranes and peroxisomes (Figure 3e,f). These results indicated the interaction of O<sub>s</sub>CV with PEX11 in peroxisomes and a role for O<sub>s</sub>CV in PEX11 turnover.

### 3.1.4 | CV expression induced a decline in number of chloroplasts, mitochondria, and peroxisomes

Chloroplasts, mitochondria, and peroxisomes are the cell organelles associated with photorespiration. WT plants grown under elevated

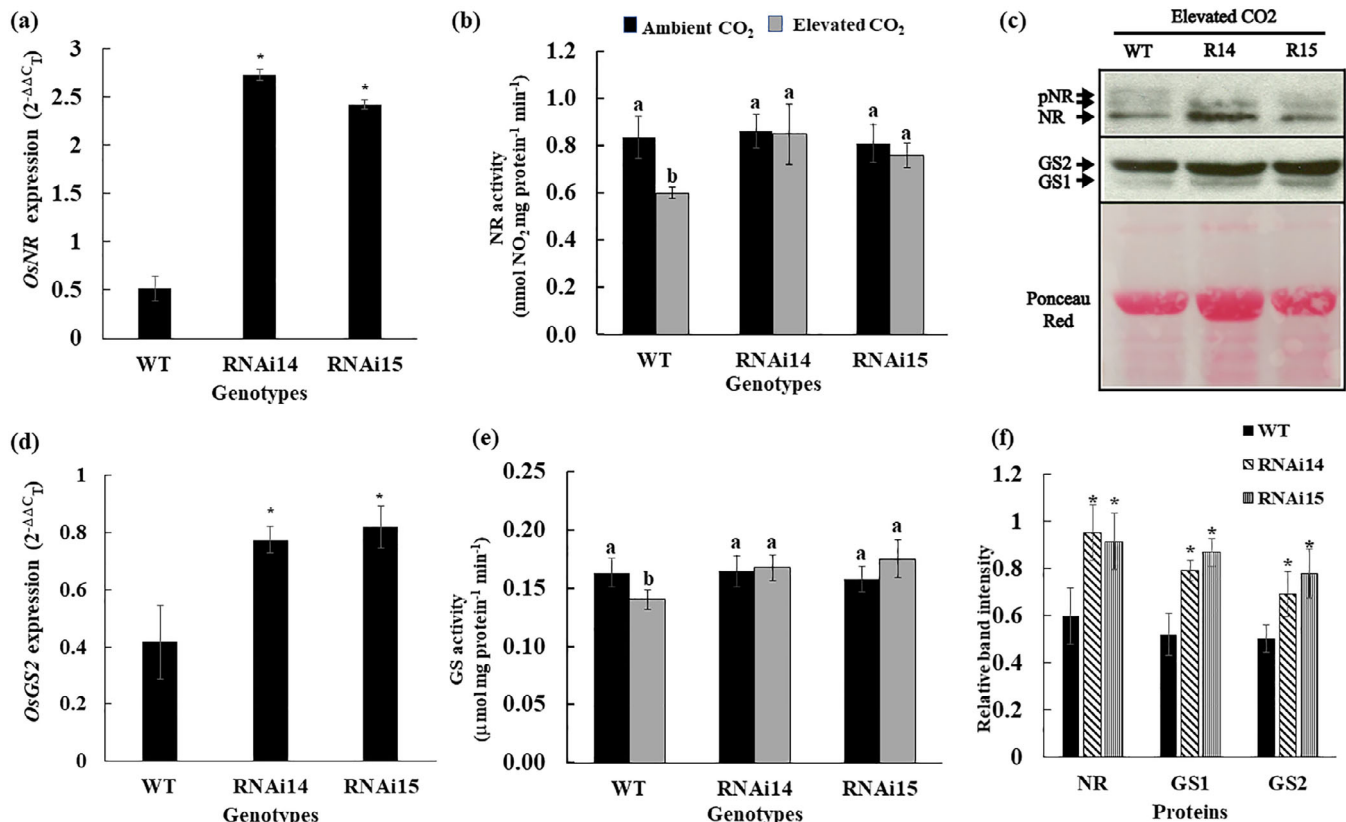


**FIGURE 5** CV-silenced rice maintained N metabolism under elevated CO<sub>2</sub>. (a, d) Relative expression of nitrate reductase (NR) and chloroplastic glutamine synthetase 2 (GS2) of wild type (WT) and RNAi-OsCV plants under elevated CO<sub>2</sub>. Values of expression at ambient conditions were normalized at 1. Values are the mean  $\pm$  standard error (SE;  $n = 5$ ). (b, e) NR activity and GS activity of WT and RNAi-OsCV plants under elevated CO<sub>2</sub>. Values are the mean  $\pm$  SE ( $n = 4$ ). (c) Western blots showing abundance of NR and GS proteins. (f) Relative intensity of bands appearing on Western blots of NR and GS. Values are the mean  $\pm$  SE ( $n = 3$ ). The asterisks indicate significant differences by Student's *t*-test ( $p \leq .05$ )

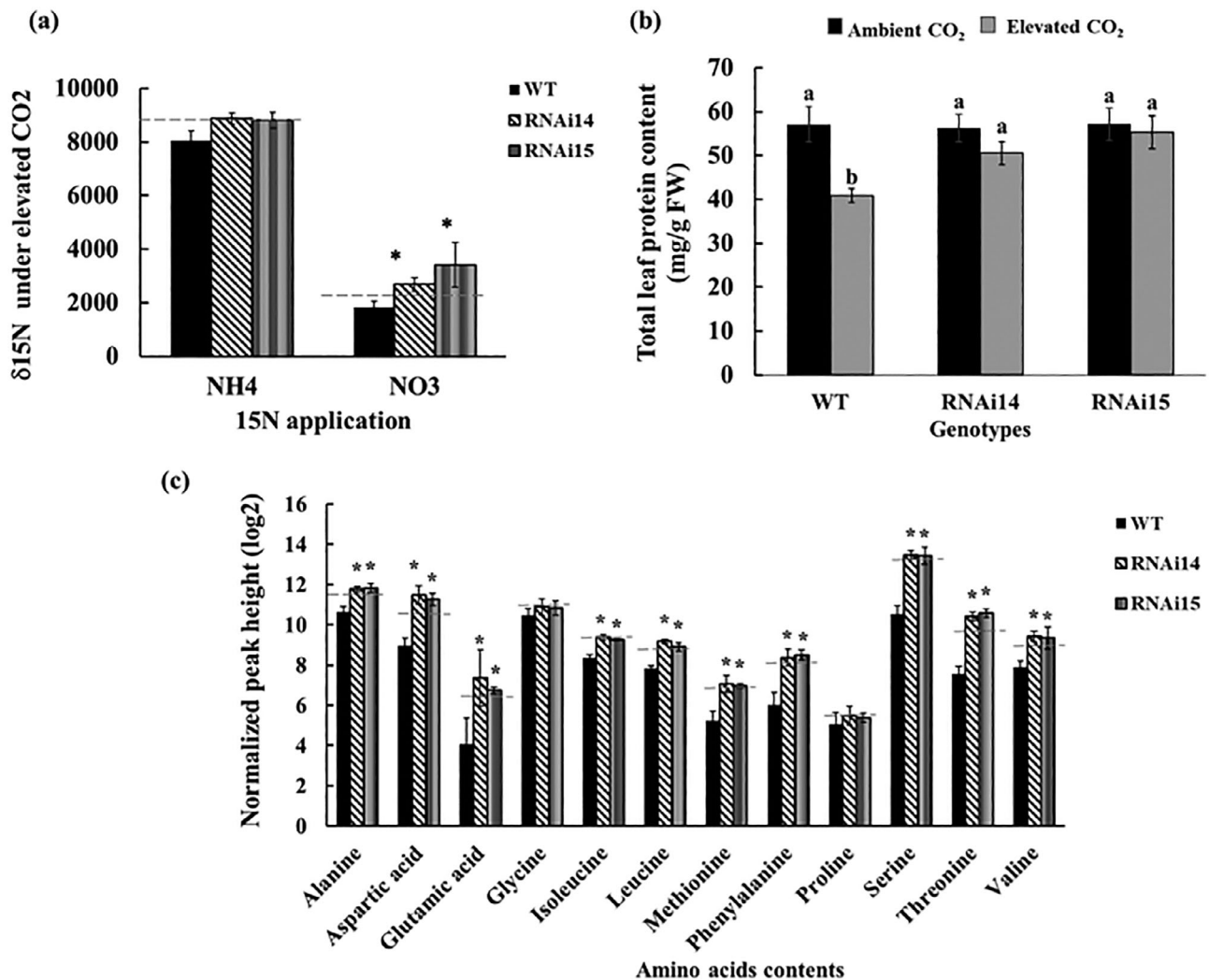


**FIGURE 6** OsCV-silenced enhanced nitrogen assimilation, total protein content, and amino acid content under elevated  $\text{CO}_2$  compared with plants grown at ambient  $\text{CO}_2$ . (a)  $\delta^{15}\text{N}$  of wild type (WT) and RNAi-OsCV, under elevated  $\text{CO}_2$  conditions. Values are the mean  $\pm$  standard error (SE) ( $n = 4-5$ ). The dashed lines represent the average  $\delta^{15}\text{N}$  contents under ambient conditions. (b) Total protein contents of WT and RNAi-OsCV plants under ambient and elevated  $\text{CO}_2$  conditions. Values are the mean  $\pm$  SE ( $n = 4$ ). (c) Amino acid contents of WT and RNAi-OsCV plants under elevated  $\text{CO}_2$ . The dashed lines represent the average amino acid contents under ambient conditions. Values are the mean  $\pm$  SE ( $n = 4$ ). The asterisks indicate significant differences from WT for each amino acid by Student's  $t$ -test ( $p \leq .05$ )

$\text{CO}_2$  displayed a significant decrease in the numbers of these three organelles (Figure 4a,c), whereas CV-silenced plants maintained the same numbers of organelles per cell as plants grown under ambient conditions (Figure 4b,c). OsCV localized to the chloroplast (Sade et al., 2018; Wang & Blumwald, 2014) and to the peroxisomes (Figure 3f,g). Natural or stress-induced senescence activated CV expression (Wang & Blumwald, 2014). CV migrated to the chloroplasts and penetrated the chloroplast envelope while disrupting the chloroplast integrity. It inserted into the thylakoid membranes, mediating the formation of vesicles that were trafficked to the vacuole, transporting the N-rich photosynthetic enzymes for proteolysis in the vacuole (Sade et al., 2018; Wang & Blumwald, 2014). In order to assess whether CV could play similar roles in the peroxisomes, we monitored

catalase activity and  $\text{H}_2\text{O}_2$  contents in plants grown under ambient and elevated  $\text{CO}_2$  concentrations (Figure 4d,f). Peroxisomes contain large amounts of catalase, an enzyme critical for the detoxification of the highly toxic  $\text{H}_2\text{O}_2$ , and the measurement of catalase activity is a good indicator of peroxisome integrity and functionality (Sheikh, Pahan, Khan, Barbosa, & Singh, 1998). CV-silenced rice plants maintained catalase activity under elevated  $\text{CO}_2$ , whereas WT plants displayed a 28% decrease in activity (Figure 4d).  $\text{H}_2\text{O}_2$ , the substrate of catalase, was also significantly higher in WT plants under elevated  $\text{CO}_2$  than in CV-silenced rice, where it remained at control levels (Figure 4e). These results indicated that consistent with the physical interaction of OsCV with OsPEX11-1, CV associated with peroxisomes under elevated  $\text{CO}_2$ ,

### 3.1.5 | Silencing CV facilitated N assimilation in plants grown under elevated CO<sub>2</sub>

Transgenic RNAi-OsCV maintained higher photorespiration and seed protein contents (Figures 1e and 2). Because photorespiration has been proposed to facilitate N assimilation (Bloom, 2015 and references therein), we examined the ability of the CV-silenced plants to assimilate nitrogen. We assessed the expression of NR and GS and NR and GS activities, the enzymes at the rate-limiting steps of NO<sub>3</sub><sup>-</sup> and NH<sub>4</sub><sup>+</sup> assimilation, respectively. Our results showed that when grown under elevated CO<sub>2</sub>, NR and GS expression was enhanced in CV-silenced rice (Figure 5a,d), which resulted in higher amounts of NR and GS proteins (Figure 5c,f) and enzymatic activities (Figure 5b,d). Using <sup>15</sup>NO<sub>3</sub><sup>-</sup> or <sup>15</sup>NH<sub>4</sub><sup>+</sup>, we observed a decrease of 10% and 25% in NO<sub>3</sub><sup>-</sup> and NH<sub>4</sub><sup>+</sup> assimilation, respectively, in WT rice plants grown under elevated CO<sub>2</sub>, but not in CV-silenced rice plants (Figure 6a), resulting in higher <sup>15</sup>NO<sub>3</sub><sup>-</sup> amounts in CV-silenced plants than in WT. The total protein contents of WT and CV-silenced rice plants grown under ambient CO<sub>2</sub> were similar, whereas WT plants showed a 30% decrease in total protein contents when grown under elevated CO<sub>2</sub> (Figure 6b). The amino acid contents of WT declined 11–38% under elevated CO<sub>2</sub>, whereas no decrease was observed for CV-silenced plants (Figure 6c).

## 4 | DISCUSSION

Atmospheric CO<sub>2</sub> has increased substantially in the last few decades (Tans & Keeling, 2018), and many questions had been raised regarding this phenomena on plant metabolism and productivity. Regarding photosynthesis, a rising concentration of atmospheric CO<sub>2</sub> is known to benefit plants by enhancing carbon fixation and plant growth (Damage et al., 2018). The primary effect of high atmospheric CO<sub>2</sub> is the increase of the CO<sub>2</sub>/O<sub>2</sub> ratio at the site of CO<sub>2</sub> fixation, increasing the carboxylation efficiency of Rubisco by lowering the rate of photorespiration (Bowes, 1991). However, productivity gains at elevated CO<sub>2</sub> are often lower than predicted (Novack et al., 2004; Easlon & Bloom, 2013; Newingham, Vanier, Charlet, & Ogle, 2013). Decreased photorespiration may be one of the main factors limiting plant productivity at high CO<sub>2</sub> concentration because of its close relationship with N assimilation (Bloom, 2015; Rachmilevitch et al., 2004).

Previously, we reported that CV silencing in rice increased source fitness, through the maintenance of chloroplast stability and N metabolism during water-deficit stress. OsCV-silenced rice plants also displayed high expression of photorespiration-associated genes under water-deficit stress (Sade et al., 2018). Because high atmospheric CO<sub>2</sub> conditions diminished photorespiration, we tested whether CV silencing might be a viable strategy to improve the effects of high CO<sub>2</sub> on grain yield and N assimilation.

OsCV-silenced plants displayed higher oxygenation rates than WT in two independent experiments (Figure 2 and Figure S1), and the higher rates were supported by the enhanced expression of photorespiration-associated genes and metabolite production

(Figure 2). Low photorespiration in the WT at elevated CO<sub>2</sub> was associated with a large change in PSII function (Figure S1b); the relative lack of change in the OsCV-silenced plants may be due to greater chloroplast stability (Sade et al., 2018). If so, it is unclear that PSII-based corrections (e.g., Bellasio et al., 2014) can be applied to improve the estimate of oxygenation. If the correction is made, then the genotype differences in oxygenation rates are diminished at elevated CO<sub>2</sub> (Figure S1c). An alternative method is based upon the assumption that all electrons passing from PSII are used in either carboxylation or oxygenation at Rubisco (Valentini et al., 1995). If oxygenation is calculated in this manner, then the OsCV-silenced RNAi15 mutant had similar rates under ambient and elevated CO<sub>2</sub>, whereas the WT did not (Figure S1d). However, the OsCV silencing change alternative electron sinks such as nitrate reduction (Figure 5), which would make the results of this method difficult to interpret.

Recently, photorespiration has been shown to be a positive regulator of growth and productivity of C3-plants, particularly under stressful conditions, where photorespiration play critical roles in several physiological processes (Busch, Sage, & Farquhar, 2018; Lopez-Calcagno et al., 2018; Rivero, Shulaev, & Blumwald, 2009). Photorespiration stimulate the assimilation of N, limited by high atmospheric CO<sub>2</sub> levels or other environmental factors (Bloom et al., 2010; Busch et al., 2018). At elevated CO<sub>2</sub>, CV-silenced rice plants displayed a higher N assimilation than WT plants. This was supported by (a) higher activity of NR and GS, key enzymes in NO<sub>3</sub><sup>-</sup> assimilation and NH<sub>4</sub><sup>+</sup> assimilation, respectively (Figure 5); (b) higher total and seed protein contents (Figures 1 and 6); and (c) <sup>15</sup>N enrichment analysis (Figure 6).

Moreover, higher malate contents in CV-silenced plants (Figure 2d) support the link between photorespiration and N assimilation. Malate can serve various purposes; in the cytosol, it can be converted into oxaloacetate to produce NADH for nitrate reduction via NR, but it can also be used to support ammonia assimilation, facilitating the import of 2-oxoglutarate into the chloroplast and the export towards the peroxisome of glutamine from the GS/GOGAT cycle, resulting in 2-oxoglutarate/glutamate exchange without a net malate import (Wingler, Lea, Quick, & Leegood, 2000; Sheibe, 2003). Under high CO<sub>2</sub> concentrations, CV-silenced plants displayed higher GS expression and GS activity than WT. It has been shown that most of the NH<sub>4</sub><sup>+</sup> being used by GS (particularly chloroplastic glutamine synthetase; GS2) is the product of NH<sub>4</sub><sup>+</sup> from photorespiration (Keys, 2006; Masclaux-Daubresse et al., 2010). The reassimilation of NH<sub>4</sub><sup>+</sup> released from photorespiration is up to 10 times higher than the primary NH<sub>4</sub><sup>+</sup> assimilation from fertilizer uptake (Oliveira, Brears, Knight, Clark, & Coruzzi, 2002). In addition, the NO<sub>3</sub><sup>-</sup> and NH<sub>4</sub><sup>+</sup> contents were not different among all genotypes and treatments (Figure S3), implying that CV silencing did not alter the ability of uptake and storage NO<sub>3</sub><sup>-</sup> and NH<sub>4</sub><sup>+</sup> in plants grown under ambient or elevated CO<sub>2</sub> but rather affected the reassimilation and incorporation of N into amino acid and proteins.

Here, we showed the direct interaction between OsCV and OsPEX11-1 in vivo (Figure 3). The OsCV/OsPEX11-1 complex was evident in the peroxisome and through its trafficking to the PVC and

the vacuole. Moreover, when OsPEX11-1 was expressed without OsCV, it remained confined to the peroxisome and did not translocate to either the PVC or the vacuole (Figure S2). Peroxisome biogenesis factors (peroxins; PEXs) are a group of proteins involved in peroxisome biogenesis, including peroxisomal matrix protein importers, peroxisomal membrane biogenesis factors, proteins involved in peroxisome proliferation, and peroxisome inheritance (Distel et al., 1996). Evidence from genetic and biochemical analyses of yeast, mammals, and plants suggested that 25 PEX proteins were required for peroxisome biogenesis (Eckert & Erdmann, 2003). PEX11-1 is involved in promoting peroxisomal proliferation and has a role in lipid catabolism (Li & Gould, 2002; Orth et al., 2007; Cui et al., 2016;). Overexpression of AtPEX11c (the closest Arabidopsis homolog to OsPEX11-1) led to an increased number of peroxisomes without any apparent phenotype, whereas RNAi-AtPEX11c showed a reduction in peroxisome number (Orth et al., 2007).

Under elevated CO<sub>2</sub>, OsCV expression was induced, and OsCV was targeted to peroxisomes where it facilitated the removal of OsPEX11-1 from the peroxisome and delivered it to the vacuole for degradation (Figure 3). This process correlated well with the reduction in the number of peroxisomes, the decreased catalase activity and the increased H<sub>2</sub>O<sub>2</sub> content in WT plants under elevated CO<sub>2</sub> (Figure 4). Both OsCV and OsPEX11-1 are membrane-bound proteins. In mammals, PEX11 proteins bound to coat protein 1 (COP1) and recruited (ADP)-ribosylation factor (ARF1), promoting membrane vesiculation (Anton et al., 2000; Passreiter et al., 1998). In plants expressing CV, CV acted as a scaffold targeting chloroplast proteins, promoting protein turnover through the formation of vesicles that mobilized the chloroplast proteins to the vacuole (Sade et al., 2018; Wang & Blumwald, 2014). Peroxisome degradation and protein turnover are mediated by the action of proteases (e.g., LON; Baker and Paudyal, 2014; Farmer et al., 2013) and autophagy-mediated, termed pexophagy (Avin-Wittenberg & Fernie, 2014; Luo & Zhuang, 2018). Co-immunoprecipitation of OsCV-interacting proteins suggested that, similar to its role in chloroplast protein turnover, OsCV acted as a scaffold, binding peroxisomal proteins, facilitating their mobilization to the vacuoles for degradation. Interestingly, autophagy related proteins or proteases were not identified among the proteins interacting with OsCV (not shown). In contrast to the CV-mediated vesicle formation during the degradation of thylakoids (Wang & Blumwald, 2014), no vesicles originating from degrading peroxisomes were detected.

It has been suggested that photorespiration is not solely regulated by the atmospheric CO<sub>2</sub> concentration or energy limitation but also by the physical association between chloroplasts, peroxisomes, and mitochondria (Oikawa et al., 2015; Rivero et al., 2009; Shai, Schuldiner, & Zalckvar, 2016). Interestingly, in addition to maintaining chloroplast stability (Sade et al., 2018) and the number of peroxisomes, CV-silenced plants also maintained a higher number of mitochondria than WT plants under elevated CO<sub>2</sub> (Figure 4). In yeast, the physical interaction between mitochondria and peroxisomes has been demonstrated, that is, Pex11/Mdm34 (Mattiazzi et al., 2015) and Pex34/Fzo1 (Shai et al., 2018). In plants, Oikawa et al. (2015) used in situ laser analysis to demonstrate the physical interaction between

chloroplasts, peroxisomes, and mitochondria. These interactions were photosynthesis-dependent, suggesting that adenosine triphosphate from chloroplasts was required to drive the movement of the organelles. Stress-induced OsCV expression promoted chloroplast turnover and the formation of CV-mediated vesicle formation at the thylakoids, mediating N-mobilization through the traffic of photosynthetic proteins to the vacuole (Wang & Blumwald, 2014). The exposure of rice plants to high atmospheric CO<sub>2</sub> induced OsCV expression. OsCV interacted directly with OsPEX11-1, increasing peroxisome turnover with the concomitant decrease in photorespiration. Notably, no CV-containing vesicles were formed from peroxisomes, suggesting differences between the mechanism(s) associated with the turnover of chloroplasts and peroxisomes. In order to assess these differences in organelle turnover and the role(s) of OsCV in regulating peroxisome proliferation, we are currently identifying membrane-bound complexes interacting with OsCV via proximity-dependent biotin labeling (Khan, Youn, Gingras, Subramanian, & Desveaux, 2018) and MS-based identification of the protein partners.

## ACKNOWLEDGEMENTS

K.U. was supported by the DPST scholarship from the Royal Thai Government. We thank the Bloom Lab, UC Davis, for sharing a high CO<sub>2</sub> growth chamber. A special thanks to undergraduate student assistants: Lin Song, Anahut Sandhu, Shlok Bhalinge, Chia Yu Kuo, and Priscilla Nai.

## ORCID

Eduardo Blumwald  <https://orcid.org/0000-0002-6449-6469>

## REFERENCES

- Aebi, H. (1984). Catalase in vivo. *Methods in Enzymology*, 105, 121–126.
- Anton, M., Passreiter, M., Lay, D., Thai, T., Gorgas, K., & Just, W. W. (2000). ARF- and coatome-mediated peroxisomal vesiculation. *Cell Biochemistry and Biophysics*, 32, 27–36.
- Avin-Wittenberg, T., & Fernie, A. R. (2014). At long last: Evidence of pexophagy in plants. *Molecular Plant*, 7, 1257–1,260.
- Bellasio, C., Burgess, S. J., Griffiths, H., & Hibberd, J. M. (2014). High throughput gas exchange screen for determining rates of photorespiration or regulation of C4 activity. *Journal of Experimental Botany*, 65, 3769–3,779.
- Bloom, A. J. (2015). Photorespiration and nitrate assimilation: A major intersection between plant carbon and nitrogen. *Photosynthesis Research*, 123, 117–128.
- Bloom, A. J., Burger, M., Asensio, J. S. R., & Cousins, A. B. (2010). Carbon dioxide enrichment inhibits nitrate assimilation in wheat and Arabidopsis. *Science*, 328, 899–904.
- Bowes, G. (1991). Growth at elevated CO<sub>2</sub>—Photosynthetic responses mediated through Rubisco. *Plant Cell and Environment*, 14, 795–806.
- Bradford, M. M. (1976). A rapid and sensitive method for the quantitation of microgram quantities of protein utilizing the principle of protein-dye binding. *Analytical Biochemistry*, 72, 248–254.
- Brumbarova, T., Le, C. T. T., & Bauer, P. (2016). Hydrogen peroxide measurement in Arabidopsis root tissue using Amplex Red. *Bio-Protocol*, 6, 1–11.
- Busch, F. A., Sage, R. F., & Farquhar, G. D. (2018). Plants increase CO<sub>2</sub> uptake by assimilating nitrogen via the photorespiratory pathway. *Nature Plants*, 4, 46–54.



- Cao, Y., Jiang, M., Xu, F., Liu, S., & Meng, F. (2017). The effects of elevated CO<sub>2</sub> (0.5%) on chloroplasts in the tetraploid black locust (*Robinia pseudoacacia* L.). *Ecology and Evolution*, 10, 546–10,555.
- Cui, P., Liu, H., Islam, F., Li, L., Farooq, M. A., Ruan, S., & Zhou, W. (2016). OsPEX11, a peroxisomal biogenesis factor 11, contributes to salt stress tolerance in *Oryza sativa*. *Frontiers in Plant Science*, 7, 1–11.
- Distel, B., Erdmann, R., Gould, S. J., Blobel, G., Crane, I. D. I., Cregg, I. J. M., ... Vennhuis, M. (1996). A unified nomenclature for peroxisome biogenesis factors. *The Journal of Cell Biology*, 135, 1–3.
- Drake, B. G., González-Meler, M. A., & Long, S. P. (1997). More efficient plants: A consequence of rising atmospheric CO<sub>2</sub>? *Annual Review of Plant Biology*, 48, 609–639.
- Dusenge, M. D., Duarte, A. G., & Way, S. A. (2018). Plant carbon metabolism and climate change: Elevated CO<sub>2</sub> and temperature impacts on photosynthesis, photorespiration and respiration. *New Phytologist*, 221, 32–49. <https://doi.org/10.1111/nph.15283>
- Earley, K. W., Haag, J. R., Pontes, O., Opper, K., Juehne, T., Song, K., & Pikaard, C. S. (2006). Gateway-compatible vectors for plant functional genomics and proteomics. *Plant Journal*, 45, 616–629.
- Easlon, H. M., & Bloom, A. J. (2013). The effects of rising atmospheric carbon dioxide on shoot-root nitrogen and water signaling. *Frontiers in Plant Science*, 4, 1–8.
- Eckert, J. H., & Erdmann, R. (2003). Peroxisome biogenesis. *Reviews of Physiology Biochemistry and Pharmacology*, 147, 75–121.
- Fan, K.-T., Rendahl, A. K., Chen, W.-P., Freund, D. M., Gray, W. M., Cohen, J. D., & Hegeman, A. D. (2016). Proteome scale-protein turnover analysis using high resolution mass spectrometric data from stable-isotope labeled plants. *Journal of Proteome Research*, 15, 851–867.
- Fiehn, O., Wohlgemuth, G., Scholz, M., Kind, T., Lee, D. Y., Lu, Y., ... Nikolau, B. (2008). Quality control for plant metabolomics: Reporting MSI-compliant studies. *Plant Journal*, 53, 691–697.
- Foresti O., Gershlick D.C., Bottanelli F., Hummel E., Hawes C. & Denecke J.A (2010) Recycling-defective vacuolar sorting receptor reveals an intermediate compartment situated between prevacuoles and vacuoles in tobacco. *The Plant Cell*, 22, 3,992–4,008, 3992, 4008.
- Gehl, C., Waadt, R., Kudla, J., Mendel, R. R., & Hänsch, R. (2009). New Gateway vectors for high throughput analyses of protein–protein interactions by bimolecular fluorescence complementation. *Molecular Plant*, 2, 1,051–1,058.
- Genty, B., Briantais, J. M., & Baker, N. R. (1989). The relationship between the quantum yield of photosynthetic electron transport and quenching of chlorophyll fluorescence. *Biochimica et Biophysica Acta*, 990, 87–92.
- Kaiser, J. J., & Lewis, O. A. M. (1984). Nitrate reductase and glutamine synthetase activity in leaves and roots of nitrate-fed *Helianthus annuus* L. *Plant and Soil*, 77, 127–130.
- Kao, Y.-T., Gonzalez, K. L., & Bartel, B. (2018). Peroxisome function, biogenesis, and dynamics in plants. *Plant Physiology*, 176, 162–177.
- Kessel-Vigeli, S. K., Wiese, J., Schroers, M. G., Wrobel, T. J., Hahn, F., & Linka, N. (2013). An engineered plant peroxisome and its application in biotechnology. *Plant Science*, 210, 232–240.
- Keys, A. J. (2006). The re-assimilation of ammonia produced by photorespiration and the nitrogen economy of C<sub>3</sub> higher plants. *Photosynthesis Research*, 87, 165–175.
- Khan, M., Youn, J.-Y., Gingras, A.-C., Subramanian, R. S., & Desveaux, D. (2018). In planta proximity dependent biotin identification (BioID). *Sci. Rep.*, 8, 9212.
- Krom, D. M. (1980). Spectrophotometric determination of ammonia: A study of a modified Berthelot reaction using salicylate and dichloroisocyanurate. *Analyst*, 105, 305–316.
- Li, X. (2011). Infiltration of *Nicotiana benthamiana* protocol for transient expression via agrobacterium. *Bio-101*, e95. <https://doi.org/10.21769/BioProtoc.95>
- Livak, K. J., & Schmittgen, T. D. (2001). Analysis of relative gene expression data using real-time quantitative PCR and the 2<sup>−(Delta Delta C [T])</sup> method. *Methods*, 25, 402–408.
- Lopez-Calcano, P. E., Fisk, S., Brown, K. L., Bull, S. E., South, P. F., & Raines, C. A. (2018). Overexpressing the H-protein of the glycine cleavage system increases biomass yield in glasshouse and field-grown transgenic tobacco plants. *Plant Biotechnology Journal*, 17, 141–151. <https://doi.org/10.1111/pbi.12953>
- Luo, M., & Zhuang, X. (2018). Selective degradation of peroxisome by autophagy in plants: Mechanisms, functions and perspectives. *Plant Science*, 274, 485–491.
- Masclaux-Daubresse, C., Daniel-Vedele, F., Dechorgnat, J., Chardon, F., Gaufichon, L., & Suzuki, A. (2010). Nitrogen uptake, assimilation and remobilization in plants: Challenges for sustainable and productive agriculture. *Annals of Botany*, 105, 1,141–1,157.
- Mattiazzi, U., Brložnik, M., Kaferle, P., Žitnik, M., Wolinski, H., Leitner, F., ... Petrovic, U. (2015). Genome-wide localization study of yeast Pex11 identifies peroxisome–mitochondria interactions through the ERMES complex. *Journal Molecular Biology*, 427, 2072–2087.
- Nelson, B. K., Cai, X., & Nebenfuhr, A. (2007). A multicolored set of in vivo organelle markers for co-localization studies in Arabidopsis and other plants. *Plant Journal*, 51, 1,126–1,136.
- Newingham, B. A., Vanier, C. H., Charlet, T. N., & Ogle, K. (2013). No cumulative effect of 10 years of elevated [CO<sub>2</sub>] on perennial plant biomass components in the Mojave Desert. *Global Change Biology*, 19, 2,168–2,181.
- Oikawa, K., Matsunaga, S., Mano, S., Kondo, M., Yamada, K., Hayashi, M., ... Nishimura, M. (2015). Physical interaction between peroxisomes and chloroplasts elucidated by in situ laser analysis. *Nature Plants*, 1, 1–12.
- Oliveira, I. C., Brears, T., Knight, T. J., Clark, A., & Coruzzi, G. M. (2002). Overexpression of cytosolic glutamine synthetase. Relation to nitrogen, light, and photorespiration. *Plant Physiology*, 129(1), 170–1,180.
- Orth, T., Reumann, S., Zhang, X., Fan, J., Wenzel, D., Quan, S., & Hu, J. (2007). The PEROXIN11 protein family controls peroxisome proliferation in Arabidopsis. *The Plant Cell*, 19, 333–350.
- Passreiter, M., Anton, M., Lay, D., Frank, R., Harter, C., Wieland, F. T., ... Just, W. W. (1998). Peroxisome biogenesis: Involvement of ARF and coatomer. *The Journal of Cell Biology*, 141, 373–383.
- Rachmilevitch, S., Cousins, A. B., & Bloom, A. J. (2004). Nitrate assimilation in plant shoots depends on photorespiration. *Proceedings of the National Academy of Sciences of the United States of America*, 101, 31.
- Reguera, M., Peleg, Z., Abdel-Tawab, Y. M., Tumimbang, E. B., Delatorre, C., & Blumwald, E. (2013). Stress-induced cytokinin synthesis increases drought tolerance through the coordinated regulation of carbon and nitrogen assimilation in rice. *Plant Physiology*, 16(1), 609–622.
- Reumann, S., & Bartel, B. (2016). Plant peroxisomes: Recent discoveries in functional complexity, organelle homeostasis, and morphological dynamics. *Current Opinion in Plant Biology*, 34, 17–26.
- Ripley, B. S., Gilbert, M. E., Ibrahim, D. G., & Osborne, C. P. (2007). Drought constraints on C<sub>4</sub> photosynthesis: Stomatal and metabolic limitations in C<sub>3</sub> and C<sub>4</sub> subspecies of *Alloteropsis semialata*. *Journal of Experimental Botany*, 58, 1,351–1,363.
- Rivero, R. M., Shulaev, V., & Blumwald, E. (2009). Cytokinin-dependent photorespiration and the protection of photosynthesis during water deficit. *Plant Physiology*, 150(15), 301–540.
- Sade, N., Umnajkitikorn, K., Rubio Wilhelmi, M. M., Wright, M., Wang, S., & Blumwald, E. (2018). Delaying chloroplast turnover increases water-deficit stress tolerance through the enhancement of nitrogen assimilation in rice. *Journal of Experimental Botany*, 69, 867–878.
- Shai, N., Schuldiner, M., & Zalckvar, E. (2016). No peroxisome is an Island—Peroxisome contact sites. *Biochimica Biophysica Acta*, 1863, 1,061–1,069.

- Shai, N., Yifrach, E., van Roermund, C. W. T., Cohen, N., Bibi, C., Ijst, L., ... Zalcvar, E. (2018). Systematic mapping of contact sites reveals tethers and a function for the peroxisome-mitochondria contact. *Nature Communications*, 9, 1761.
- Sheikh F. G., Pahan K., Khan M., Barbosa E. & Singh I. (1998) Abnormality in catalase import into peroxisomes leads to severe. *Proceedings of the National Academy of Sciences of the United States of America*, 95, 2,961–2,966, 2961, 2966.
- Shipman-Roston, R. L., Ruppel, N. J., Damoc, C., Phinney, B. S., & Inoue, K. (2010). The significance of protein maturation by plastidic type I signal peptidase 1 for thylakoid development in Arabidopsis chloroplasts. *Plant Physiology*, 152, 1,297–1,308.
- Tamaki, H., Reguera, M., Abdel-Tawab, Y. M., Takebayashi, Y., Kasahara, H., & Blumwald, E. (2015). Targeting hormone-related pathways to improve grain yield in rice: A chemical approach. *PLoS One*, 10, e0131213.
- Tans, P., & Keeling, R. (2016). *Trends in atmospheric carbon dioxide [online]*. Mauna Loa, Hawaii: NOAA. <http://www.esrl.noaa.gov/gmd/ccgg/trends>
- Teng, N., Wang, J., Chen, T., Wu, X., Wang, Y., & Lin, J. (2006). Elevated CO<sub>2</sub> induces physiological, biochemical and structural changes in leaves of *Arabidopsis thaliana*. *New Phytologist*, 172, 92–103.
- Thompson, M., Gamage, D., Hirotsu, N., Martin, A., & Saman, S. (2017). Effects of elevated carbon dioxide on photosynthesis and carbon partitioning: A perspective on root sugar sensing and hormonal crosstalk. *Frontiers in Physiology*, 8, 578.
- Timm, S., Florian, A., Wittmiß, M., Jahnke, K., Hagemann, M., Fernie, A. R., & Bauwe, H. (2013). Serine acts as a metabolic signal for the transcriptional control of photorespiration-related genes in Arabidopsis. *Plant Physiology*, 162, 379–389.
- Uemura, T., Tomonari, Y., Kashiwagi, K., & Igarashi, K. (2004). Uptake of GABA and putrescine by UGA4 on the vacuolar membrane in *Saccharomyces cerevisiae*. *Biochemical Biophysical Research Communication*, 315, 1,082–1,087.
- Valentini, R., Epron, D., Angelis, P., Matteucci, G., & Dreyer, E. (1995). *In situ* estimation of net CO<sub>2</sub> assimilation, photosynthetic electron flow and photorespiration in Turkey oak (*Q. cerris* L.) leaves: Diurnal cycles under different levels of water supply. *Plant, Cell & Environment*, 18, 631–640.
- Voss, I., Sunil, B., Scheibe, R., & Raghavendra, A. S. (2013). Emerging concept for the role of photorespiration as an important part of abiotic stress response. *Plant Biology*, 15, 713–722.
- Wang, S., & Blumwald, E. (2014). Stress-induced chloroplast degradation in Arabidopsis is regulated via a process independent of autophagy and senescence-associated vacuoles. *The Plant Cell*, 26, 4,875–4,888.
- Weckwerth, W., Wenzel, K., & Fiehn, O. (2004). Process for the integrated extraction, identification and quantification of metabolites, proteins and RNA to reveal their co-regulation in biochemical networks. *Proteomics*, 4, 78–83.
- Wingler, A., Lea, P. J., Quick, W. P., & Leegood, R. C. (2000). Photorespiration: Metabolic pathways and their role in stress protection. *Philosophical Transactions of the Royal Society B*, 355, 1,517–1,529.

### SUPPORTING INFORMATION

Additional supporting information may be found online in the Supporting Information section at the end of this article.

**How to cite this article:** Umnajkitikorn K, Sade N, Rubio Wilhelmi MM, Gilbert ME, Blumwald E. Silencing of OsCV (*chloroplast vesiculation*) maintained photorespiration and N assimilation in rice plants grown under elevated CO<sub>2</sub>. *Plant Cell Environ*. 2020;1–14. <https://doi.org/10.1111/pce.13723>